nature chemical biology

Article

https://doi.org/10.1038/s41589-024-01778-z

Detecting features of antibody structure through their mediator-accessible redox activities

Received: 9 May 2023

Accepted: 22 October 2024

Published online: 02 December 2024

Check for updates

Dana Motabar[1,2,3], Eunkyoung Kim[2,3], Jinyang Li[1,2,3], Zhiling Zhao[2,3], Trina Mouchahoir[2,4], D. Travis Gallagher[2,4], John E. Schiel[2,4], Mamatha Garige[5], Carole Sourbier[5], Gregory F. Payne[2,3] ✉ & William E. Bentley[1,2,3] ✉

Protein function relies on sequence, folding and post-translational modification and molecular measurements are commonly used to reveal these structural features. Here, we report an alternative approach that represents these molecular features as readily measurable electronic patterns and validate this experimental approach by detecting structural perturbations commonly encountered during protein biomanufacturing. We studied a monoclonal antibody standard (from the National Institute of Standards and Technology) and focused on the electronic detection of variants that have undergone interchain disulfide bond reduction and methionine oxidation. Electronic detection of these structural perturbations is based on mediated electrochemical probing (MEP) that discerns patterns associated with the antibody's mediator-accessible redox activity. We demonstrate that MEP can rapidly (within minutes) and quantitatively detect alterations in the antibody's structural features and produce robust electronic signals that could enable monitoring of biomanufacturing processes. The ability to transduce information regarding a protein's structural perturbations into a more convenient electronic domain offers opportunities to apply the power of microelectronics and real-time data analytics to chemical and biological analysis.

The amino acid sequence of proteins encodes information regarding their structure, folding and post-translational modifications. Commonly, the amino acids undergo redox (reduction–oxidation)-based modifications by redox-active molecules (for example, reactive oxygen species), which can impact protein structure and function. In some cases, these post-translational redox modifications may be essential to biological structure and function (for example, thiol-to-disulfide sulfur switching of cysteine residues)[1–4] or detrimental (for example, oxidative damage)[5–7].

Here, we report a rapid method to detect features of protein structure through their mediator-accessible redox activities (MARA) and we use therapeutic monoclonal antibodies (mAbs), as our model. Therapeutic antibodies have an important role in human health (therapeutics and diagnostics) and account for a substantial portion of global sales revenue for all biopharmaceutical products[8–10]. Throughout their development and manufacture, mAbs can be altered by redox reactions resulting in interchain disulfide bond reduction or

[1]Fischell Department of Bioengineering, University of Maryland, College Park, MD, USA. [2]Institute for Bioscience and Biotechnology Research, Rockville, MD, USA. [3]Robert E. Fischell Institute for Biomedical Devices, University of Maryland, College Park, MD, USA. [4]National Institute of Standards and Technology, Gaithersburg, MD, USA. [5]Laboratory of Molecular Oncology, Division of Biotechnology Review and Research-I, Office of Biotechnology Products, Office of Pharmaceutical Quality, Center for Drug Evaluation and Research (CDER), US Food and Drug Administration (FDA), Silver Spring, MD, USA. ✉e-mail: gpayne@umd.edu; bentley@umd.edu

https://doi.org/10.1038/s41589-024-01778-z

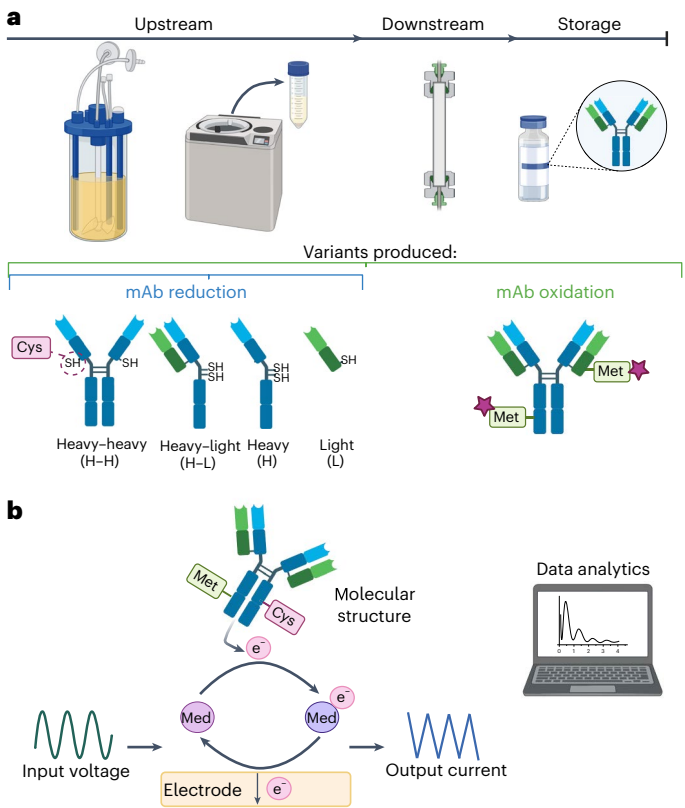

Fig. 1 | MEP to detect mAb variants. a, During manufacturing and storage, redox reactions can yield mAb reduction and oxidation variants. **b**, MEP measures the mAb's MARA and allows information of protein structure to be converted into a convenient electronic format.

methionine oxidation, which dramatically affect therapeutic efficacy, quality and safety[11–13].

As illustrated in Fig. 1a, antibody reduction is a common upstream bioprocessing issue that has been observed both in the bioreactor and during centrifugal harvest[14–16]. Reduction of the antibody's disulfide bonds leads to lower-molecular-weight forms (containing free sulfhydryl groups), impacting product stability, bioactivity and downstream process performance[13,17]. Irreversible oxidation of methionine residues can occur at all stages of bioprocessing and storage because of exposure to light, oxygen or metal ions. Methionine oxidation also alters product quality and pharmacokinetic profiles[18,19]. Redox-based modifications are closely monitored to ensure optimal production, patient safety and approval by the Food and Drug Administration (FDA)[20].

Importantly, tools that enable access to redox-based biological information are critical. Gold-standard analytical methods (for example, mass spectrometry (MS) and capillary electrophoresis (CE)) provide highly detailed chemical information that enables the comprehensive and robust characterization of mAbs. However, these technologies tend to be expensive and labor intensive; they may also require lengthy processing times. As such, it is well recognized that new process analytical methodologies are needed for therapeutic mAb production[21,22], specifically those that allow for rapid, sensitive and convenient measurement and that can serve as a complement to more traditional analytical methods. These methodologies should provide ready access to key process information so that they can be incorporated into advanced control schemes. We suggest that electrochemical measurements using electrodes are ideal for this purpose; sterilizable pH and dissolved oxygen electrochemical probes, for example, are standard measurement tools in bioprocessing because of their reliability, ease of use and ability to connect to electronics.

Here, we extend an emerging electrochemical method, mediated electrochemical probing (MEP)[23–26], for the simple, rapid and sensitive detection of mAb reduction and oxidation variants. As illustrated in Fig. 1b, this method probes the mAb-containing sample using a diffusible redox mediator and an electrode with a precisely imposed voltage input sequence. In our case, the mediator is oxidized at the electrode and then diffuses into the sample where it probes the mAb for oxidizable residues. Among the most important in mAbs are cysteine residues that confer structural integrity through their ability to form disulfide bonds linking adjacent fragments. Importantly, while cysteine residues are often buried within the three-dimensional structure of a protein, cysteines in mAb are often exposed and this enables their redox reaction. In a reduced fragment, exposed thiols of the cysteine residues are oxidizable by the mediator, leaving the mediator in a reduced state. Thus, the MARA of the mAb is detected when the reduced mediator returns to the electrode and its redox state is measured. Information of the mAb's MARA is, thus, embedded in the electronic output features that are assessed using data analytics and comparative analysis[27,28]. In this way, simple addition of mediators whose redox potential enables reaction with accessible redox-active residues can be detected by simply measuring current at the appropriate applied potential. Experimentally, we demonstrate the detection of reduced protein thiols (cysteine) and oxidized sulfur residues (methionine) using a standard reference material (National Institute of Standards and Technology (NIST) mAb reference material 8671) and a commercial product, durvalumab. Overall, we believe that this work demonstrates that mediated electrochemistry allows complex molecular information (for example, of protein structure) to be rapidly converted into an electronic format that, in turn, enables broad application for on-site, remote and deployable analysis.

Results

Reduction probing the model amino acid, cysteine

To demonstrate MEP, in Fig. 2, we show how cysteine, one of the most important redox-sensitive molecular 'switches' in biological systems, can be electrochemically characterized. When antibodies undergo reduction, the disulfide bonds are disrupted and cysteine thiol groups are exposed. Our method leverages the exposed thiol groups to discern when the antibody is reduced. The scheme in Fig. 2a describes the proposed reaction mechanism for oxidative redox cycling between the redox mediator ferrocene dimethanol (Fc) and cysteine. Fc was chosen as the mediator as it is a weak oxidant that is selective for exposed cysteines; it is too mild to oxidize other amino acid residues (that is, lysine and tyrosine), as shown in our previous work[29]. In MEP, redox mediators (acting as electron shuttles) are added to biological samples, which then interact with redox-active elements through the exchange of electrons[27,30]. When the appropriate input voltage is applied, Fc is oxidized by the electrode (Fc^{Ox}), diffuses away from the electrode surface and exchanges electrons with cysteine. This redox cycling reaction regenerates the reduced form (Fc^{Red}) because of the transfer of electrons from cysteine, resulting in an amplification in the oxidative current relative to the mediator alone in solution. Conversely, in the second panel of Fig. 2a, attenuation in the reductive current occurs because of the decrease in availability of Fc^{Ox}. The choice of mediator, Fc, is ideally suited for probing the oxidation state of cysteine as it can redox cycle (amplify the signal) at slightly oxidizing potentials (relative to cysteine), has a well-defined electrochemical signal and is easily quantified.

As illustrated in Fig. 2b, Fc-mediated oxidation of cysteine can be measured using either of two electrochemical methods with distinct voltage input schemes, cyclic voltammetry (CV) or chronocoulometry (CC). For CV, as shown with the Fc (50 μmol L^{-1}) control, the input potential was scanned in the forward (positive) direction, which led to an oxidative peak ($Fc^{Red} \rightarrow Fc^{Ox} + e^-$), and then scanned in the reverse (negative) direction, which led to a reductive peak ($Fc^{Ox} + e^- \rightarrow Fc^{Red}$). The Fc

https://doi.org/10.1038/s41589-024-01778-z

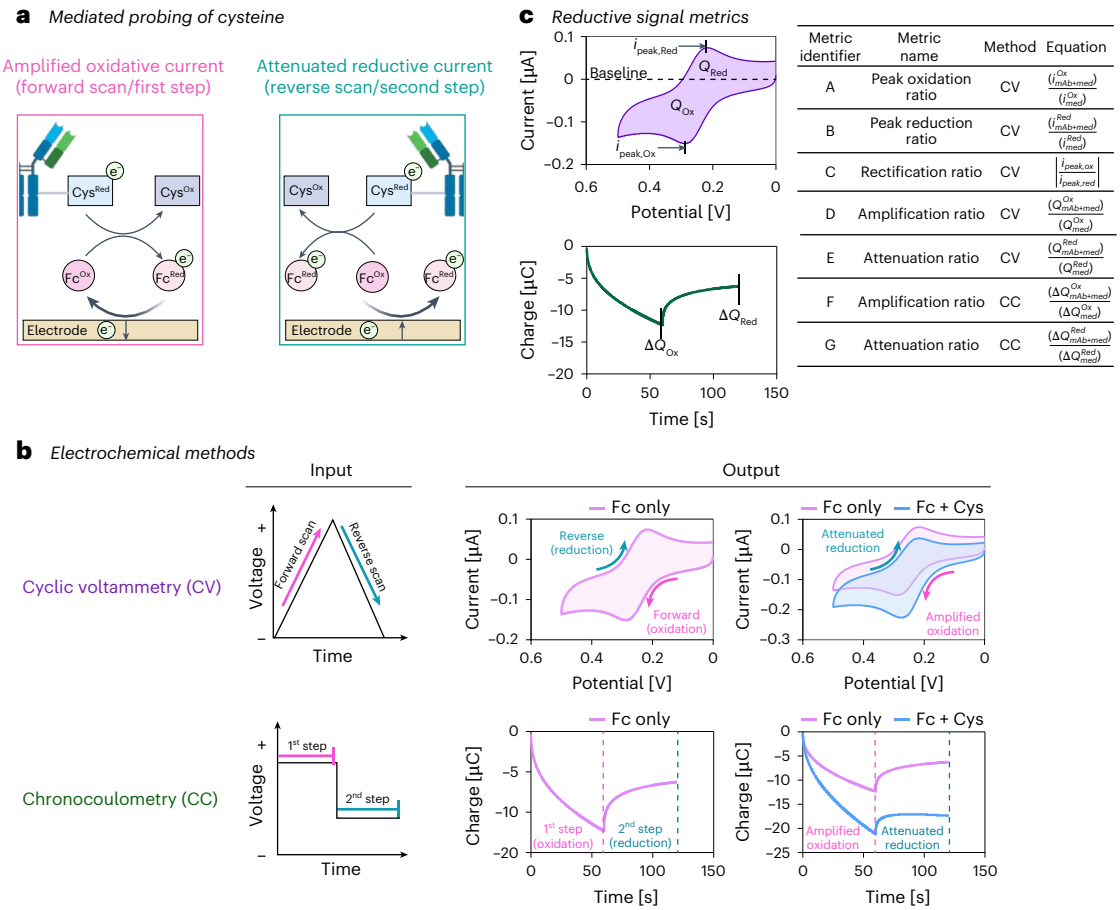

Metric identifier	Metric name	Method	Equation
A	Peak oxidation ratio	CV	$\frac{(i^{Ox}_{mAb+med})}{(i^{Ox}_{med})}$
B	Peak reduction ratio	CV	$\frac{(i^{Red}_{mAb+med})}{(i^{Red}_{med})}$
C	Rectification ratio	CV	$\left\lvert\frac{i_{peak,ox}}{i_{peak,red}}\right\rvert$
D	Amplification ratio	CV	$\frac{(Q^{Ox}_{mAb+med})}{(Q^{Ox}_{med})}$
E	Attenuation ratio	CV	$\frac{(Q^{Red}_{mAb+med})}{(Q^{Red}_{med})}$
F	Amplification ratio	CC	$\frac{(\Delta Q^{Ox}_{mAb+med})}{(\Delta Q^{Ox}_{med})}$
G	Attenuation ratio	CC	$\frac{(\Delta Q^{Red}_{mAb+med})}{(\Delta Q^{Red}_{med})}$

Fig. 2 | Mediated probing of cysteine. a, Proposed reaction mechanism during Fc-mediated redox cycling. **b**, CV and CC plots of mediated probing of cysteine (50 μmol L^{-1}) with Fc (50 μmol L^{-1}). **c**, Plots and table describing the reductive signal metrics for quantitative analysis.

reaction is electrochemically reversible as evidenced by the oxidation and reduction peak currents having a potential separation (80 mV) that is relatively similar to that of the expected value (approximately 60 mV) for a reversible one-direction electron transfer reaction[31]. For CC, the applied potential is fixed but the principle is the same: quantification of the current generated by redox reactions occurring at the applied voltage. Here, the first voltage input was a 1-min step change to an oxidative value, which oxidized Fc (+0.4 V versus Ag–AgCl), and the second voltage input was a 1-min step change to a reductive value, which reduced the oxidized Fc (+0.1 V versus Ag–AgCl). When cysteine (50 μmol L^{-1}) was added to Fc (50 μmol L^{-1}), the CV and CC responses were dramatically altered as compared to the Fc controls. Specifically, the oxidative responses were greatly amplified and the reductive responses were attenuated, following from Fig. 2a. When reduced cysteine is present, Fc oxidized at the electrode exchanges electrons with cysteine, becomes reduced and then returns to the electrode to be oxidized. The current generated is the oxidative peak. The reaction with cysteine (reactive sink) enables greater current generated by Fc–electrode interactions than in the absence of cysteine, as shown in the controls.

Importantly, because both CV and CC have characteristic shapes and are highly reproducible, signal metric analyses can be applied to quantitatively analyze the data. We suggest that this is analogous to the assessment of cardiac function with electrocardiogram (EKG) measurements in which electrodes are used to discern a signature pattern that characterizes the health and functioning of the heart[32]. Figure 2c lists the parameters and calculations by which our metrics are defined. For CV, the oxidative and reductive charges (Q_{Ox} or Q_{Red}) were defined as the area under the curve (AUC) below and above the zero-current baseline, respectively. The oxidative and reductive peak currents ($i_{peak,ox}$ or $i_{peak,red}$) are the minima and maxima of the CV peak currents, respectively. For CC, the oxidative charge (ΔQ_{Ox}) is defined as the change in the charge after the first minute and the reductive charge (ΔQ_{Red}) is defined as the difference between the charges of the first and second minutes. Metrics based on the amplification of the oxidative response were expected to increase (that is, metrics A, C, D and F) in the presence of reduced cysteine because of the free thiol content, whereas metrics based on the attenuation of the reductive response were expected to decrease (that is, metrics B, E and G). For brevity, the metrics are later referred to by their identifier (metrics A–G, Fig. 2c).

Detection of antibody reduction using MEP

Next, we investigated the ability of MEP to evaluate the MARA of proteins. We selected NISTmAb as a test case because of its relevance as a reference standard in the biopharmaceuticals industry. NISTmAb oxidation and reduction, for example, are well studied using a variety of techniques and reference protocols[33]. To evaluate states that might be produced during biomanufacturing[15–17,34], we intentionally reduced NISTmAb using TCEP (Methods and Supplementary Fig. 1) to generate reduction variants and used these to provide samples of known quantities. In this way, we could systematically evaluate our protocol for structural information of the lower-molecular-weight species (light, heavy, light–heavy and heavy–heavy), where free thiols are generated from the broken disulfide linkages of the otherwise intact antibody[35].

Ellman's assay and microchip CE were used to characterize antibody reduction. Using these methods, we first verified that our treated samples were indeed reduced. Details are provided in the

https://doi.org/10.1038/s41589-024-01778-z

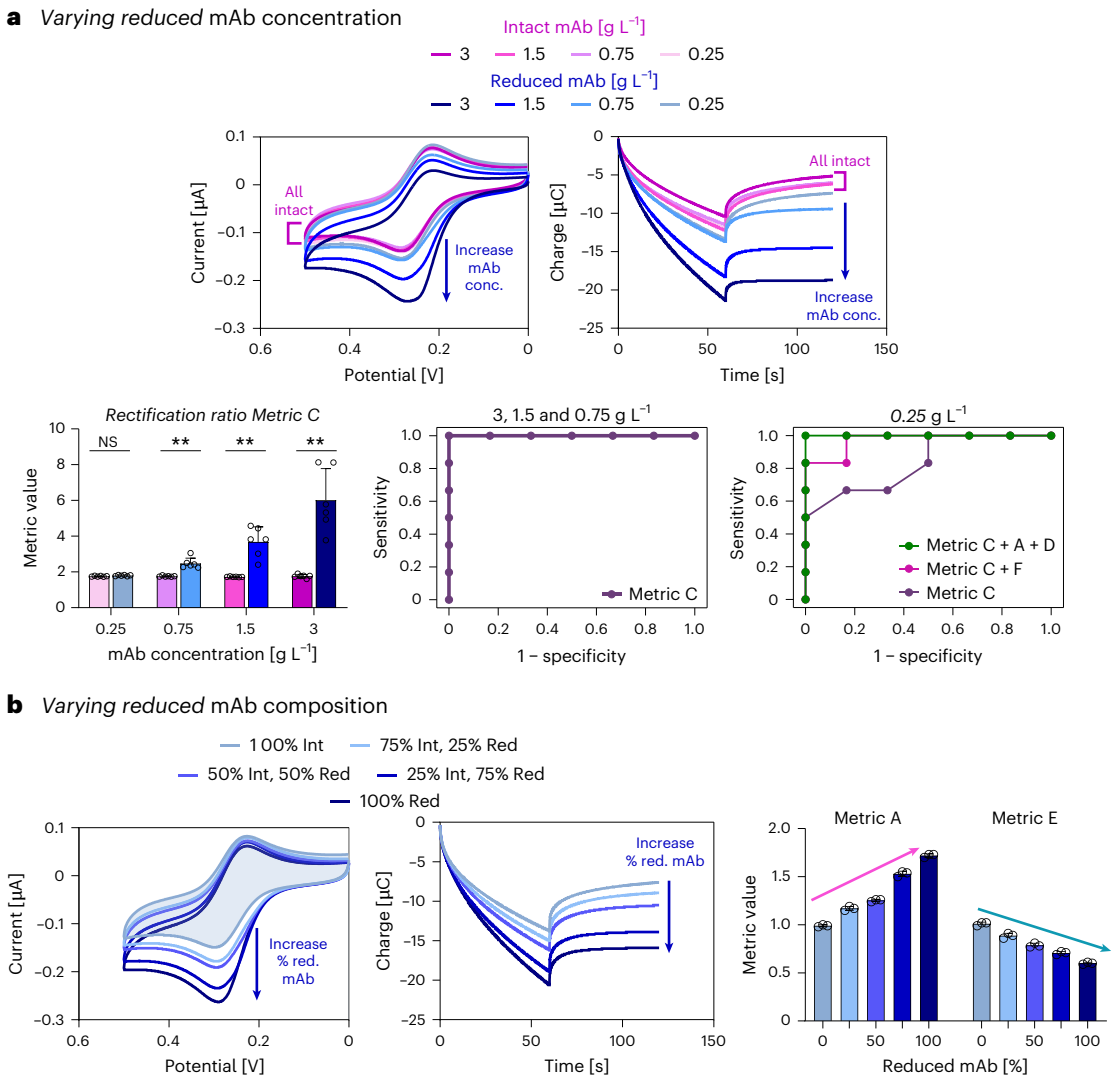

Fig. 3 | Varying reduced mAb concentration and composition. a, Representative CV and CC of intact and reduced mAb at different concentrations: 3, 1.5, 0.75 and 0.25 g L^{-1} ($n = 6$). Corresponding signal metric bar graph and ROC curves. Data were analyzed using the Mann–Whitney two-tailed test (bar graph) and a logistic regression model (ROC plot). For the bar graph, statistical significance is defined as $^{*}P \leq 0.05$ and $^{**}P \leq 0.01$; NS (not significant), $P > 0.05$. Exact P values are as follows: 3 g L^{-1}, 0.0037; 1.5 g L^{-1}, 0.0041; 0.75 g L^{-1}, 0.0650; 0.25 g L^{-1}, 0.02. For the ROC curve of 0.25 g L^{-1} NISTmAb, the discriminatory power of the model increased as additional metrics were combined: metric C, AUC = 0.833; metrics C + F, AUC = 0.972; metrics C + A + D, AUC = 1.000. **b**, Representative CV and CC plots of ratios of intact to reduced mAb (total mAb, 3 g L^{-1}; $n = 3$ replicates): 100% intact, 75% intact–25% reduced, 50% intact–50% reduced, 25% intact–75% reduced and 100% reduced. The corresponding plot of best fit signal metrics is shown. Data are presented as the mean values ± s.d.

Supplementary Information. In brief, Ellman's assay (Supplementary Fig. 1b) confirmed the presence of free thiol groups in the reduced samples across all concentrations evaluated (3, 1.5, 0.75 and 0.25 g L^{-1}). Importantly, the increase in mAb concentration was directly correlated with increased free thiol content. Microchip CE (Supplementary Fig. 1c) was also used to evaluate free heavy-chain and light-chain monomers and intermediate species generated upon antibody reduction. The non-reduced CE results demonstrated that the reduction protocol was effective as there was minimal intact mAb and high levels of fully reduced heavy and light chains. Importantly, these data confirm that the reduction of NISTmAb resulted in free-thiol-containing antibody fragments that are structurally similar to those produced in bioprocessing settings because of interchain disulfide bond reduction[16,17,34].

For electrochemical analysis, Fc (50 µmol L^{-1}) was added to intact and reduced NISTmAb samples. As shown in the CV and CC plots of Supplementary Fig. 2a, we first determined that there were no notable alterations in the electrochemical responses of the Fc mediator in the presence of intact mAb (Fc versus Fc + intact). In Supplementary Fig. 2b, we show that the reduction protocol had no independent influence from residual TCEP[36]. The top panels of Fig. 3a show the results of MEP analysis of Fc (50 µmol L^{-1}) mixed with a range of industrially relevant NISTmAb concentrations (3, 1.5, 0.75 and 0.25 g L^{-1}). As expected, we observed that the intact mAb responses (that is, pink shades) remained essentially unchanged across all concentrations evaluated. This indicates that there was no Fc-mediated electron exchange with NISTmAb in its native form. The electrochemical 'silence' of the intact NISTmAb is consistent with expectations that (1) there are no mediator-accessible cysteine residues and (2) Fc is too weak an oxidant to react with other surface-accessible amino acid residues. In contrast, for the reduced mAb, we observed (1) redox cycling between Fc and the reduced mAb, as noted by increased oxidative current and decreased reductive current at the peak potentials, and (2) higher oxidative amplification and reductive attenuation as the reduced mAb concentration increased. The concentration-dependent alterations in the CV and CC responses can be correlated with the free thiol content of the samples (Supplementary Fig. 1b, table). Independent MS analysis of Fc-mediated cysteine

https://doi.org/10.1038/s41589-024-01778-z

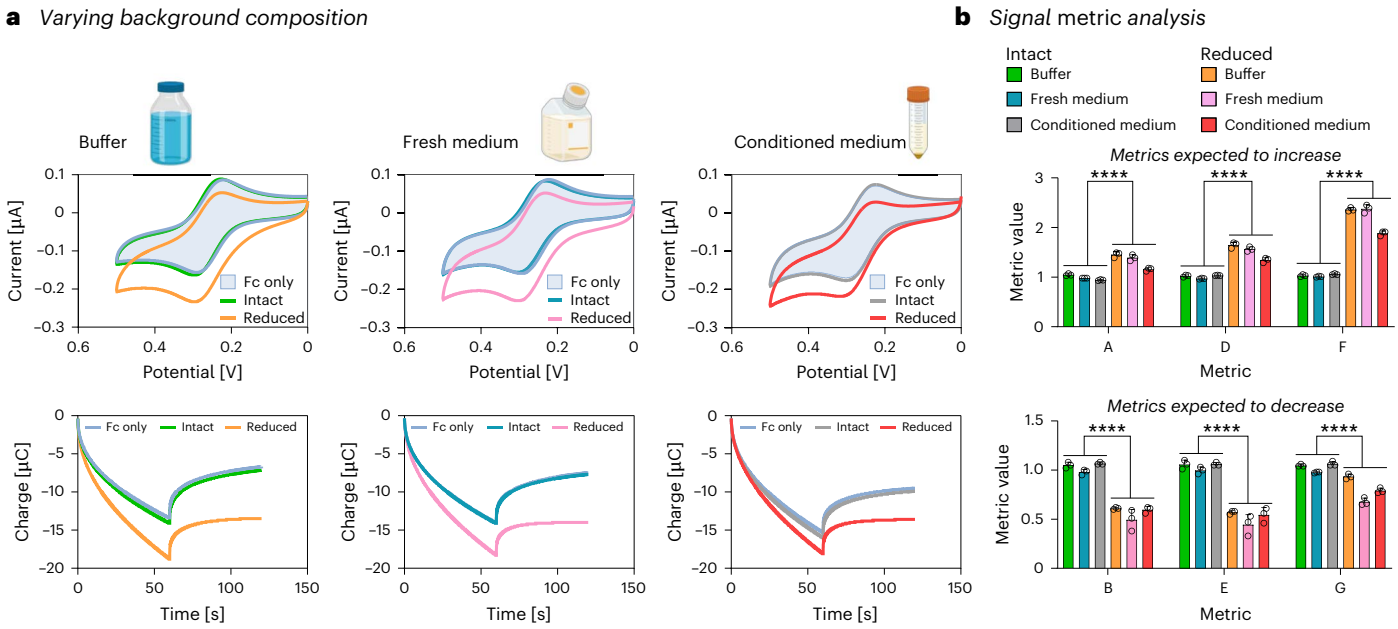

Fig. 4 | Reduced mAb in different background conditions. a, Representative CV and CC plots of intact and reduced mAb, which were diluted in a 1:1 ratio with PBS, fresh medium or conditioned medium (total mAb, 2 g L^{-1}) ($n = 3$). **b**, Signal metric analysis showing that MEP can significantly discern intact from reduced mAb over all conditions tested. Data were analyzed using the Mann–Whitney two-tailed test; statistical significance defined as $^{****}P \leq 0.0001$. Exact P values for all tests were <0.0001. Data are presented as the mean values ± s.d.

oxidation indicated the formation of cysteine rather than any other oxygenated forms (for example, sulfenic, sulfonic and sulfinic acids)[29]. Furthermore, MS and CV data from other redox-active residues such as lysine and tyrosine showed no redox interaction with Fc, confirming the specificity of Fc to exchange electrons with cysteine[29].

We applied signal metric analyses to further confirm that observed differences between intact and reduced mAbs were statistically significant. First, the Mann–Whitney test was used to evaluate whether the calculated metrics for the two groups were distinct ($n = 6$ for both groups). In the bar graphs of Fig. 3a, metric C provided clear discriminatory power among all samples at higher concentrations (3, 1.5 and 0.75 g L^{-1}). Furthermore, we found that all the calculated metrics enabled powerful discrimination, particularly at the higher concentrations (Supplementary Fig. 3a). Supplementary Figure 3b shows that simple linear regression analyses revealed concentration dependence ($R^2 \geq 0.95$) for all metrics across all concentrations. Interestingly, we also found no correlation with intact mAb for nearly all metrics (outliers: metrics E and G), which is consistent with the earlier result that Fc does not redox cycle with intact mAb, presumably because it has no surface-accessible cysteine residues.

Akin to evaluating cardiovascular function wherein several metrics of an EKG are combined for comprehensive understanding, we applied a logistic regression model[37] to evaluate combinations of metrics to further increase the probability of discriminating between intact and reduced forms. Akaike information criterion (AIC) values were used to assess the goodness of fit, while receiver operating characteristic (ROC) curves with the AUC and P values were used to assess the discriminating power. In Fig. 3a, at higher mAb concentrations (3, 1.5 and 0.75 g L^{-1}), a single metric (metric C) was sufficient to discriminate between intact and reduced samples (AUC = 1). However, combining metrics increased the AUC and the statistical significance (P value) of the analysis such that even the lowest mAb concentration (0.25 g L^{-1}) could be discriminated. That is, when three metrics were used cooperatively (metrics C, A and D), the discriminating power improved (AUC = 1). Complete analyses are shown in Supplementary Fig. 4.

We next tested the hypothesis that MEP can distinguish between intact and reduced mAb in samples comprising varied concentrations of reduced and intact mAb. That is, we wanted to check whether the detection of reduced mAb was influenced by the intact form. To assess, Fc (50 µmol L^{-1}) was added to NISTmAb mixed in the following ratios: 100% intact, 75% intact–25% reduced, 50% intact–50% reduced, 25% intact–75% reduced and 100% reduced (total mAb for all samples, 3 g L^{-1}). Representative CV and CC plots are shown in Fig. 3b. As the percentage composition of reduced mAb increased, the oxidative response was amplified and the reductive response was attenuated, as anticipated. Clear linear trends were revealed for metrics A and E (additional metrics shown in Supplementary Fig. 5a). Upon further examination (Supplementary Fig. 5b), we found not only that MEP metrics could distinguish intact from reduced mAb but also that the results were concentration dependent and virtually all metrics showed linearity across the full range of mAb concentrations evaluated.

Importantly, it would expand the usefulness of our methodology if samples could be analyzed in conditions where interfering components may be present. In bioprocessing settings, mAbs are in cell culture medium containing vitamins, amino acids and other potentially redox-active components. To evaluate the degree to which the matrix affects our assay, NISTmAb (in PBS) was diluted in a 1:1 ratio (total mAb, 2 g L^{-1}) with PBS, fresh medium (Advanced Mammalian Biomanufacturing Innovation Center (AMBIC) basal medium 1.1) or conditioned medium (spent Ex-Cell advanced fed-batch medium from Chinese hamster ovary cell cultivations). CV and CC plots (Fig. 4a) suggest that MEP consistently discerned between intact and reduced mAbs in each process setting. Signal metrics analyses (Fig. 4b) further indicated that, for all conditions, all oxidative response metrics were observed to increase and all reductive response metrics decreased, as anticipated. While the discriminatory power of MEP was shown to be independent of the solution background, it is important to note that sample conditions do impact the magnitude of the electrochemical responses. For example, the reduced mAb in conditioned medium had slightly lower values for metrics A, D and F compared to samples in buffer or fresh medium. Overlaid CV plots of samples in different backgrounds (Supplementary Fig. 6) show how redox-active components contribute to the CV or CC spectra as 'signature' patterns deviate mainly from the Fc spectrum and less so from the blank solutions (denoted 'background'). Not shown

https://doi.org/10.1038/s41589-024-01778-z

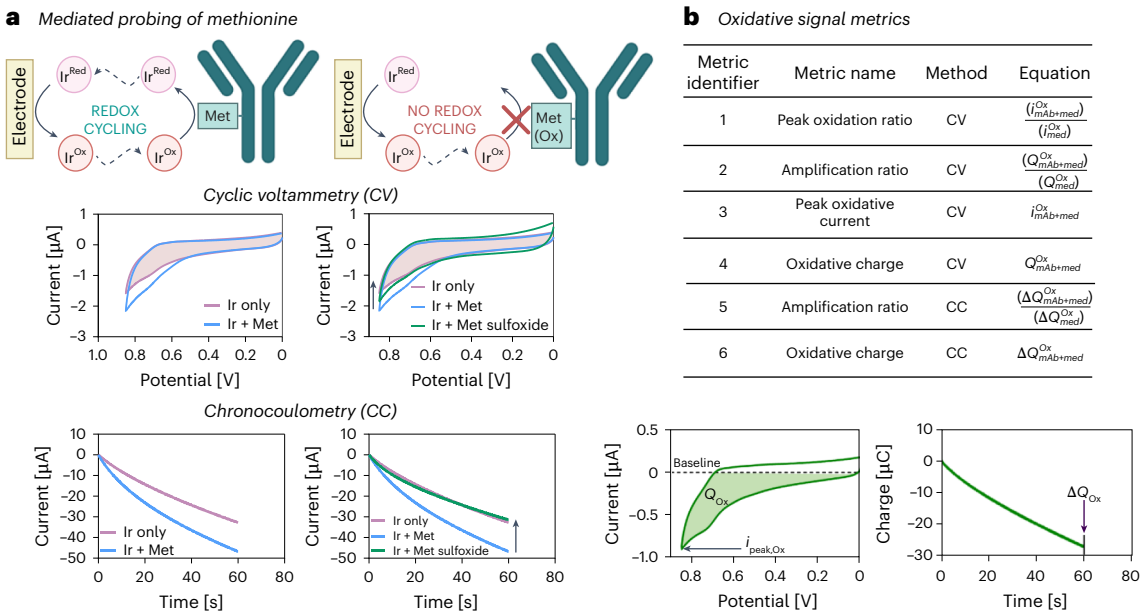

Metric identifier	Metric name	Method	Equation
1	Peak oxidation ratio	CV	$\frac{(i^{Ox}_{mAb+med})}{(i^{Ox}_{med})}$
2	Amplification ratio	CV	$\frac{(Q^{Ox}_{mAb+med})}{(Q^{Ox}_{med})}$
3	Peak oxidative current	CV	$i^{Ox}_{mAb+med}$
4	Oxidative charge	CV	$Q^{Ox}_{mAb+med}$
5	Amplification ratio	CC	$\frac{(\Delta Q^{Ox}_{mAb+med})}{(\Delta Q^{Ox}_{med})}$
6	Oxidative charge	CC	$\Delta Q^{Ox}_{mAb+med}$

Fig. 5 | MEP of methionine. a, Ir (50 µmol L^{-1}) redox cycles with methionine (2 mmol L^{-1}). Ir does not cycle with the oxidized form of methionine (methionine sulfoxide; 2 mmol L^{-1}). **b**, CV and CC plots along with corresponding table describing the oxidative signal metrics for quantitative analysis.

are data from many experiments of varied mediator concentration, electrode material and analyte concentration used to determine the most effective conditions, as discussed below.

In sum, by quantifying electrochemical features, calculating metrics and statistically assembling their significance, MEP enables the rapid and statistically valid assessment of mAb reduction.

Oxidation probing the model amino acid, methionine

Analogously to targeting cysteine, we wanted to establish that MEP interacts with the primary target of antibody oxidation, methionine. Recognizing that methionine has a higher redox potential than cysteine, the redox mediator hexachloroiridate(IV) (Ir) was used because it is a stronger oxidant than Fc (+0.67 V for Ir versus +0.25 V for Fc) and it can target the sulfur of methionine. Figure 5a describes the proposed reaction mechanism between Ir and methionine using MEP; when Ir (50 µmol L^{-1}) is added to methionine (2 mmol L^{-1} methionine; Ir + Met), redox cycling occurs, resulting in a great amplification in the oxidative response for both CV and CC measurements (most notable at potentials above 0.6 V). When methionine is oxidized (2 mmol L^{-1} methionine sulfoxide added to buffer) and, therefore, electron deficient, redox cycling no longer occurs and the oxidative response reverts to a level similar to that of the Ir control. In turn, Ir has no discernable reductive peak at these potentials. These data establish that Ir can redox cycle with methionine but not with oxidized methionine (no electron exchange). Hence, only oxidative signal metrics were applied to quantitatively analyze the results, potentially limiting discrimination. The CV and CC plots in Fig. 5b illustrate the parameters by which the metrics were defined. For CV, the oxidative charge (Q_{Ox}) was defined as the AUC below the no current baseline and the peak oxidative current ($i_{peak,ox}$) was defined as the maximum peak in the oxidative region. For CC, the potential was stepped to +0.85 V for 1 min, which oxidizes Ir and is defined as the oxidative charge (ΔQ_{Ox}). The table (Fig. 5b, bottom) defines the equations and identifiers (1–6) of the metrics.

Detection of antibody oxidation using mediated probing

We next investigated the ability of MEP to discern between control (nonoxidized) and oxidized mAbs. As before, we used NISTmAb and treated NISTmAb with a protocol for altering its oxidative state. We also examined durvalumab, a clinically relevant immunotherapeutic. For oxidation of NISTmAb (Supplementary Fig. 7a), hydrogen peroxide (1% v/v) was added to the mAb (4 g L^{-1}) and incubated in the dark for 48 h. This treatment was previously used at NIST to assess NISTmAb oxidation and preferentially oxidizes solvent-exposed methionine residues[38–40]. Samples were then buffer-exchanged into PBS before further analysis. Oxidation of the antibody's methionine residues (identified for NISTmAb in Supplementary Fig. 7b) was confirmed by liquid chromatography (LC)–MS/MS peptide mapping. In brief, Supplementary Fig. 7c reveals that six methionine residues (heavy chain M34, M101, M255, M361 and M431; light chain M4) showed significant oxidation (>95 %). The remaining two residues (heavy chain M87 and light chain M32) were only partially oxidized (<7 %), likely because of their limited solvent accessibility, as described in the solvent-accessible surface area (SASA) analysis (Supplementary Fig. 7d). That is, we expect that the MARA assessed by MEP would reveal features among residues that are solvent accessible. Durvalumab was identically oxidized and LC–MS/MS peptide mapping results (Supplementary Fig. 7e) indicate that three of the five methionine residues (heavy chain M256, M362 and M432) were significantly oxidized (>97 %) while the two remaining residues (heavy chain M34 and M83) were only partially oxidized (<3 %). Overall, these data confirm that the methionine residues of NISTmAb and durvalumab were oxidized because of incubation with hydrogen peroxide.

For electrochemical analysis, control and oxidized NISTmAb and durvalumab samples were diluted to 0.25 g L^{-1}, mixed with Ir (50 µmol L^{-1}), and assayed as above. In Supplementary Fig. 8a, the oxidative response of the intact mAb (Ir + intact) was amplified compared to the mediator by itself (Ir only). This demonstrates that Ir redox cycles with the surface-exposed redox-active amino acids. The results from the CV and CC measurements for control and oxidized NISTmAb (Fig. 6a) reveal that oxidized mAb exhibited a decreased oxidative response compared to control mAb. While less dramatic, these data are consistent with the methionine results.

Mann–Whitney tests and logistic regression models were applied to evaluate the characteristic metrics. For the Mann–Whitney test, shown in the bar graphs of Fig. 6a and Supplementary Fig. 8b, all metrics exhibited significantly different responses ($P \leq 0.05$ and $^{**}P \leq 0.01$). We note, however, that a higher number of replicates were required to achieve these differences (CV: $n = 20$ and CC: $n = 15$ versus $n = 6$ for mAb reduction

https://doi.org/10.1038/s41589-024-01778-z

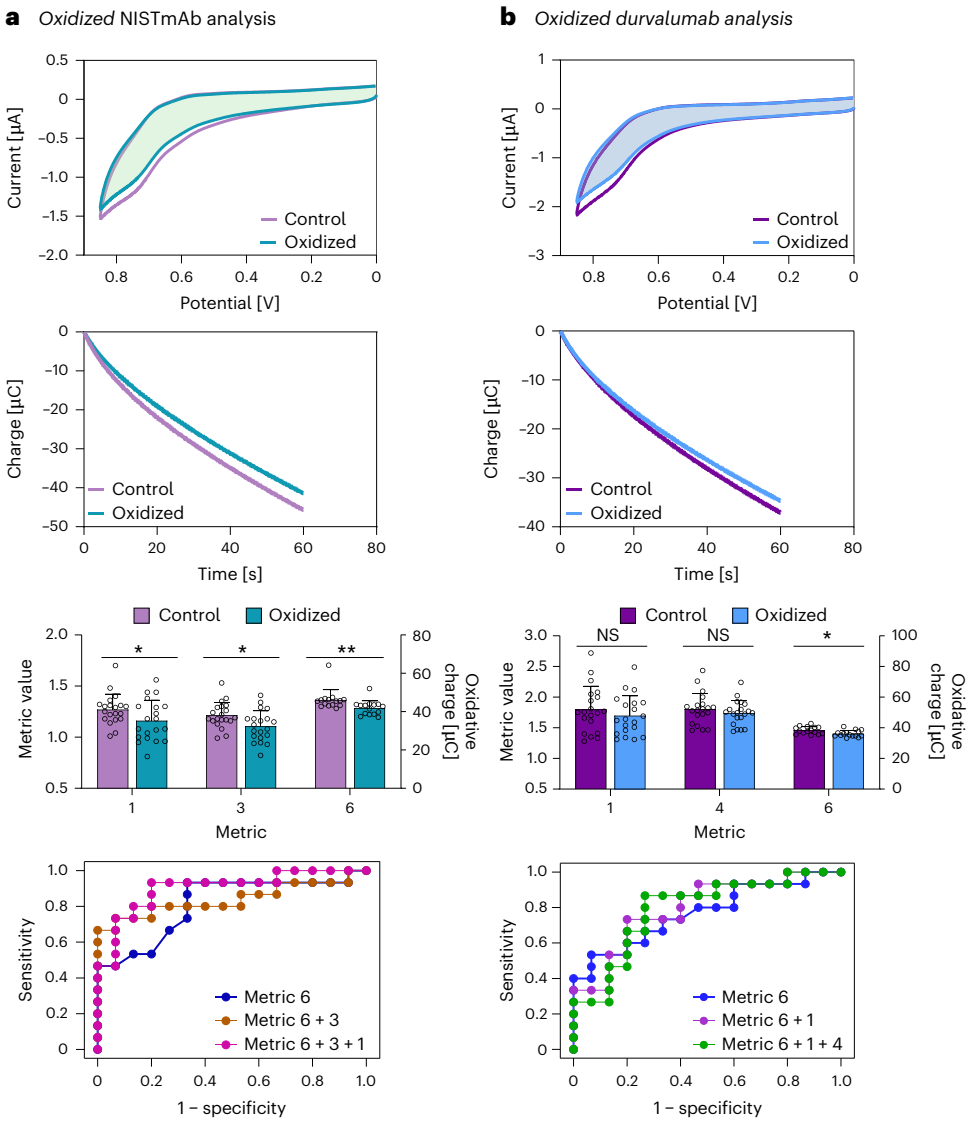

Fig. 6 | MEP of oxidized mAbs. a, MEP of control and oxidized NISTmAb (0.25 g L^{-1}). For the ROC plot, the discriminatory power of the model increased as additional metrics were combined: metric 6, AUC = 0.813; metrics 6 + 3, AUC = 0.840; metrics 6 + 3 + 1, AUC = 0.902. **b**, MEP of control and oxidized durvalumab (0.25 g L^{-1}). Both mAbs were probed with Ir (50 µmol L^{-1}) using CV (n = 20) and CC (n = 15) techniques. For the ROC plot, the combination of two metrics provided the optimal discriminatory power: metric 6, AUC = 0.771; metrics 6 + 1, AUC = 0.796; metrics 6 + 1 + 4, AUC = 0.791. For bar charts, statistical significance is defined as *$P \leq 0.05$ and **$P \leq 0.01$; NS, $P > 0.05$. Exact P values for NISTmAb are as follows: metric 1, 0.0480; metric 3, 0.0197; metric 6, 0.0089. Exact P values for durvalumab are as follows: metric 1, 0.3724; metric 4, 0.3795; metric 6, 0.0102. Data were analyzed using the Mann–Whitney two-tailed test (bar graph) and a logistic regression model (ROC plot). Data are presented as the mean values ± s.d.

studies). The logistic model again indicated that combinations of metrics increased resolving power (Fig. 6a, ROC plot, and Supplementary Fig. 8c, table). Here, a combination of multiple metrics (1, 3 and 6) increased the discriminating power of MEP for evaluating mAb oxidation.

As noted above, the mediator and mAb concentrations are important for effective MEP analysis. In Supplementary Fig. 9, we varied the NISTmAb concentration (62.5, 125, 250 and 500 mg L^{-1}) while maintaining the same Ir concentration (50 µmol L^{-1}). Conversely, we also maintained the NISTmAb concentration (250 mg L^{-1}) while varying the Ir concentration (25, 50, 75 and 100 µmol L^{-1}). We then quantitatively evaluated our data by applying select metrics (metrics 1 and 2, which appeared most distinguishing). In both cases, we found that the same conditions (125 and 250 mg L^{-1} NISTmAb and 50 µmol L^{-1} Ir) resulted in the largest difference between control and oxidized samples. That is, at several other NISTmAb–Ir concentrations and ratios, we were unable to differentiate control from oxidized samples.

For durvalumab, which had three oxidized methionine residues in a heavy–light chain pair (Supplementary Fig. 10a), using the identical concentrations as NISTmAb, we observed that the oxidative response of the control mAb (Ir + control) was also amplified compared to the mediator by itself (Ir only). Results for metrics 1, 4 and 6 are shown in Fig. 6b. Like NISTmAb, oxidized durvalumab had a lower average oxidative response compared to the intact protein in both CV and CC measurements. The statistical analysis, shown in the bar graphs of Fig. 6b and Supplementary Fig. 10b, with the Mann–Whitney test (using the same number of CV and CC replicates as NISTmAb) revealed that, although the metrics trended as expected, only metric 6 had a statistically significant difference ($P \leq 0.05$) between the groups. Interestingly, metric 6 also yielded the highest significant difference ($P \leq 0.01$) for NISTmAb. For the logistic model, as displayed in Supplementary Fig. 10c (ROC plot and table), the combination of two metrics (metrics 6 + 1) improved the ability to distinguish between control and oxidized

durvalumab (AUC = 0.796), while the addition of a third metric (metrics 6 + 1 + 4) had minimal impact (AUC = 0.791).

Discussion

A protein's functional attributes (for example, activity and immunogenicity) are intimately linked to structure; thus, measurements are integral to protein characterization. The challenge, however, is that protein structure extends over various length scales (from sequence to quaternary structure); thus, structural characterization often requires multiple methods of analysis (for example, MS and X-ray crystallography). While these gold-standard methods are essential for establishing structure–function relationships, they are slow and require specialized skills, making them difficult to adapt for near-real-time information that is often essential for decision-making in a biomanufacturing environment. Here, we report the use of MEP as an alternative; it rapidly converts a protein's structural information (for example, quaternary structural alterations because of interchain disulfide bond reduction) directly into an electronic format. Specifically, MEP uses mediators and a precisely controlled potential (that is, voltage) inputs to probe a protein's MARA and generates output response signals (that is, currents) that can be correlated to relevant structural features. In essence, it provides an electronic signature of the accessible redox residues; for proteins such as antibodies, these residues (typically containing sulfur) are of pivotal importance as they often reflect structural variants.

First, we used the standard reference protein, NISTmAb, and examined how MEP with a thiol-targeting mediator, Fc, could be used to detect partially reduced variants generated by interchain disulfide bond reduction. We observed that the weakly oxidative Fc redox mediator can selectively detect the free thiols of cysteine residues and, when variants with higher thiol contents were probed, stronger MEP-based current responses were shown (Fig. 3a,b). Importantly, the reduction of mAb disulfides that yields free thiols also results in partial dissociation of protein subunit chains. Thus, the MEP-based detection of free thiols in the reduced variants is also a measure of the loss of the mAb's native quaternary structure. Second, we observed that MEP was able to discern between intact and reduced samples in the presence of interfering analytes (for example, buffer, fresh medium and conditioned medium). As shown in Fig. 4, signal metrics trended similarly for samples in all three conditions. This is a major advantage of the MEP methodology as it can lower the processing time and effort required to detect reduced mAb, especially by lowering the number of time-consuming steps required for sample preparation. While our focus was the detection of molecular perturbations to protein structure, we expect that these measurements could be extended to quantitative (or semiquantitative) analysis because the intact mAb showed no signal upon Fc mediator probing while the reduced mAb showed concentration-dependent changes in signal metrics.

Similarly, we used MEP to probe partially oxidized antibody variants using both NISTmAb and durvalumab. In this case, we used a more strongly oxidative mediator, Ir, that can detect methionine's oxidation. First, we showed that MEP detected statistically significant differences between the partially oxidized (versus unoxidized) mAbs and these differences appeared correlated to solvent-exposed methionine residues that are common sites of mAb oxidation. Figure 6a,b indicate that the lower significance in the differences between the oxidized and unoxidized mAb for durvalumab (versus NISTmAb) may be related to the smaller number of oxidized methionine residues (three for durvalumab and six for NISTmAb in a heavy–light chain pair). Importantly, these results suggest that the MEP methodology is sensitive to the amino acid composition of proteins. Second, we observed that the detection of mAb oxidation variants was more challenging (than detecting reduction variants) and required greater experimental optimization and more extensive logistic regression analysis to increase the discerning power of the MEP-generated signals. Perhaps this is because of the number of MARA cysteine versus methionine residues in intact mAbs.

Overall, this work demonstrates the potential of MEP to convert information of molecular structure into a convenient electronic format. There are two important practical implications of this work. First, MEP measurements are made using simple, inexpensive and miniaturizable electrodes that can be deployed in manufacturing settings. Our specific example is relevant to the biomanufacturing of mAbs where we envision that MEP could enable a new, device-based process analytical technology[21]. Second, MEP provides near-real-time electronic data that allow instantaneous statistical analysis and decision-making. Thus, we envision that MEP can provide timely, actionable information of molecular structure that will eventually enable product-based process control in a biomanufacturing setting.

Online content

Any methods, additional references, Nature Portfolio reporting summaries, source data, extended data, supplementary information, acknowledgements, peer review information; details of author contributions and competing interests; and statements of data and code availability are available at https://doi.org/10.1038/s41589-024-01778-z.

References

1. Poole, L. B. The basics of thiols and cysteines in redox biology and chemistry. *Free Radic. Biol. Med.* **80**, 148–157 (2015).
2. Paulsen, C. E. & Carroll, K. S. Cysteine-mediated redox signaling: chemistry, biology, and tools for discovery. *Chem. Rev.* **113**, 4633–4679 (2013).
3. Georgiou, G. How to flip the (redox) switch. *Cell* **111**, 607–610 (2002).
4. Paulsen, C. E. & Carroll, K. S. Orchestrating redox signaling networks through regulatory cysteine switches. *ACS Chem. Biol.* **5**, 47–62 (2010).
5. Sies, H., Berndt, C. & Jones, D. P. Oxidative stress. *Annu. Rev. Biochem.* **86**, 715–748 (2017).
6. Halliwell, B. Biochemistry of oxidative stress. *Biochem. Soc. Trans.* **35**, 1147–1150 (2007).
7. Berlett, B. S. & Stadtman, E. R. Protein oxidation in aging, disease, and oxidative stress. *J. Biol. Chem.* **272**, 20313–20316 (1997).
8. Lu, R.-M. et al. Development of therapeutic antibodies for the treatment of diseases. *J. Biomed. Sci.* **27**, 1–30 (2020).
9. Ecker, D. M., Jones, S. D. & Levine, H. L. The therapeutic monoclonal antibody market. *MAbs* **7**, 9–14 (2015).
10. Walsh, G. & Walsh, E. Biopharmaceutical benchmarks 2022. *Nat. Biotechnol.* **40**, 1722–1760 (2022).
11. Sinharoy, P., McFarland, K. S., Majewska, N. I., Betenbaugh, M. J. & Handlogten, M. W. Redox as a bioprocess parameter: analytical redox quantification in biological therapeutic production. *Curr. Opin. Biotechnol.* **71**, 49–54 (2021).
12. Liu, H., Nowak, C., Shao, M., Ponniah, G. & Neill, A. Impact of cell culture on recombinant monoclonal antibody product heterogeneity. *Biotechnol. Prog.* **32**, 1103–1112 (2016).
13. Ren, T. et al. Antibody disulfide bond reduction and recovery during biopharmaceutical process development—a review. *Biotechnol. Bioeng.* **118**, 2829–2844 (2021).
14. Handlogten, M. W., Wang, J. & Ahuja, S. Online control of cell culture redox potential prevents antibody interchain disulfide bond reduction. *Biotechnol. Bioeng.* **117**, 1329–1336 (2020).
15. Handlogten, M. W., Zhu, M. & Ahuja, S. Glutathione and thioredoxin systems contribute to recombinant monoclonal antibody interchain disulfide bond reduction during bioprocessing. *Biotechnol. Bioeng.* **114**, 1469–1477 (2017).
16. Trexler-Schmidt, M. et al. Identification and prevention of antibody disulfide bond reduction during cell culture manufacturing. *Biotechnol. Bioeng.* **106**, 452–461 (2010).
17. Chung, W. K. et al. Effects of antibody disulfide bond reduction on purification process performance and final drug substance stability. *Biotechnol. Bioeng.* **114**, 1264–1274 (2017).

18. Wang, W. et al. Impact of methionine oxidation in human IgG1 Fc on serum half-life of monoclonal antibodies. *Mol. Immunol.* **48**, 860–866 (2011).
19. Folzer, E. et al. Selective oxidation of methionine and tryptophan residues in a therapeutic IgG1 molecule. *J. Pharm. Sci.* **104**, 2824–2831 (2015).
20. Kaplon, H., Chenoweth, A., Crescioli, S. & Reichert, J. M. Antibodies to watch in 2022. *MAbs* **14**, 2014296 (2022).
21. Hinz, D. C. Process analytical technologies in the pharmaceutical industry: the FDA's PAT initiative. *Anal. Bioanal. Chem.* **384**, 1036–1042 (2006).
22. Guidance for industry: PAT—a framework for innovative pharmaceutical development, manufacturing and quality assurance. Available at https://www.fda.gov/media/71012/download (Food and Drug Administration, 2004).
23. Kim, E. et al. Redox probing for chemical information of oxidative stress. *Anal. Chem.* **89**, 1583–1592 (2017).
24. Kang, M. et al. Reliable clinical serum analysis with reusable electrochemical sensor: toward point-of-care measurement of the antipsychotic medication clozapine. *Biosens. Bioelectron.* **95**, 55–59 (2017).
25. Kang, M. et al. Reverse engineering to characterize redox properties: revealing melanin's redox activity through mediated electrochemical probing. *Chem. Mater.* **30**, 5814–5826 (2018).
26. Wang, Y., Liu, Y., Kim, E., Li, B. & Payne, G. F. Electrochemical reverse engineering to probe for drug–phenol redox interactions. *Electrochim. Acta* **295**, 742–750 (2019).
27. Motabar, D., Li, J., Payne, G. F. & Bentley, W. E. Mediated electrochemistry for redox-based biological targeting: entangling sensing and actuation for maximizing information transfer. *Curr. Opin. Biotechnol.* **71**, 137–144 (2021).
28. Zhao, Z. et al. Mediated electrochemical probing: a systems-level tool for redox biology. *ACS Chem. Biol.* **16**, 1099–1110 (2021).
29. Li, J. et al. Mediated electrochemistry to mimic biology's oxidative assembly of functional matrices. *Adv. Funct. Mater.* **30**, 2001776 (2020).
30. Liu, Y. et al. Connecting biology to electronics: molecular communication via redox modality. *Adv. Healthc. Mater.* **6**, 1700789 (2017).
31. Elgrishi, N. et al. A practical beginner's guide to cyclic voltammetry. *J. Chem. Educ.* **95**, 197–206 (2018).
32. Li, J. et al. Electrochemical reverse engineering: a systems-level tool to probe the redox-based molecular communication of biology. *Free Radic. Biol. Med.* **105**, 110–131 (2017).
33. Morgan, T. E. et al. Inline electrochemical reduction of NISTmAb for middle-up subunit liquid chromatography–mass spectrometry analysis. *Analyst* **146**, 6547–6555 (2021).
34. Kao, Y. H., Hewitt, D. P., Trexler-Schmidt, M. & Laird, M. W. Mechanism of antibody reduction in cell culture production processes. *Biotechnol. Bioeng.* **107**, 622–632 (2010).
35. Liu, H., Chumsae, C., Gaza-Bulseco, G., Hurkmans, K. & Radziejewski, C. H. Ranking the susceptibility of disulfide bonds in human IgG1 antibodies by reduction, differential alkylation, and LC–MS analysis. *Anal. Chem.* **82**, 5219–5226 (2010).
36. Santarino, I. B., Oliveira, S. C. B. & Oliveira-Brett, A. M. Protein reducing agents dithiothreitol and tris(2-carboxyethyl)phosphine anodic oxidation. *Electrochem. Commun.* **23**, 114–117 (2012).
37. Kim, E. et al. Association of acute psychosocial stress with oxidative stress: evidence from serum analysis. *Redox Biol.* **47**, 102138 (2021).
38. Sjöberg, B., Foley, S., Cardey, B., Fromm, M. & Enescu, M. Methionine oxidation by hydrogen peroxide in peptides and proteins: a theoretical and Raman spectroscopy study. *J. Photochem. Photobiol. B* **188**, 95–99 (2018).
39. Agrawal, N. J. et al. Prediction of the hydrogen peroxide-induced methionine oxidation propensity in monoclonal antibodies. *J. Pharm. Sci.* **107**, 1282–1289 (2018).
40. Balakrishnan, G., Barnett, G. V., Kar, S. R. & Das, T. K. Detection and identification of the vibrational markers for the quantification of methionine oxidation in therapeutic proteins. *Anal. Chem.* **90**, 6959–6966 (2018).

Methods

Materials

NISTmAb RM8671 (lot 14HB-D-002, humanized IgG1κ) was obtained from the NIST. Durvalumab (MedImmune, AstraZeneca) was purchased from McKesson Specialty Health. Fc was purchased from Santa Cruz Biotechnology. Trizma HCl and Trizma base (collectively, Tris), guanidine HCl, EDTA, iodoacetamide (IAM), urea, recombinant porcine trypsin, K_2IrCl_6 and PBS (pH 7.4) were purchased from Sigma-Aldrich. L-Histidine monohydrochloride monohydrate and L-histidine were purchased from Avantor. Formic acid (0.1%) was purchased from Honeywell. The 5 mmol L^{-1} stock solutions of Fc and K_2IrCl_6 were prepared in PBS and aliquots were stored at −20 °C. TCEP bond breaker solution, Zeba spin desalting columns (7-kDa molecular weight cutoff (MWCO)), Slide-A-Lyzer Dialysis Cassettes (10-kDa MWCO), DTNB (Ellman's Reagent) and DTT were purchased from Thermo Fisher Scientific. AMBIC basal medium 1.1 (Lonza) was provided by AMBIC.

Antibody reduction protocol

NISTmAb samples (10 g L^{-1} stock) were first diluted to 5 g L^{-1} with PBS (pH 7.4). For reduced samples, TCEP was added to 1 ml of NISTmAb (5 or 10 g L^{-1}) to a final TCEP concentration of 10 mmol L^{-1}. The intact and reduced samples were then incubated for 4 h at room temperature. Both intact and reduced samples were then dialyzed using Slide-A-Lyzer dialysis cassettes (0.5–3 mL, 10-kDa MWCO) in 2 L of PBS (pH 7.4) overnight at 4 °C. After dialysis, samples were stored at −20 °C until analysis. Buffer controls were also produced to confirm there was interference on the electrochemical signal from the buffer. Buffer controls were generated using 25 mmol L^{-1} histidine buffer (pH 6.0; NISTmAb formulation buffer) with and without the addition of TCEP. The controls were then dialyzed and diluted with PBS (pH 7.4) in an identical manner to experimental samples. Finally, buffer controls for intact and reduced mAb (Supplementary Fig. 2b) verified that the TCEP was effectively removed and that the background responses among the samples were similar. TCEP is known to have has its own electrochemical signature[41] and these data illustrate its absence after dialysis.

Determination of antibody reduction by standard approaches

To analyze antibody reduction, microchip CE was performed using a 2100 Bioanalyzer (Agilent). Intact and reduced NISTmAb samples were run using the Agilent Protein 230 kits under nonreducing conditions according to the manufacturer's protocols. A sulfhydryl assay was performed to determine free thiol content in reduced antibody samples. Briefly, 625 µl of reaction buffer (0.1 mol L^{-1} sodium phosphate and 1 mmol L^{-1} EDTA, pH 8) was mixed with 12.5 µl of 4 mg ml^{-1} of DTNB solution (in reaction buffer). Then, 62.5 µl of intact or reduced NISTmAb (3, 1.5, 0.75 and 0.25 g L^{-1}; dilutions were made with PBS) was added to the mixture and samples were then incubated for 15 min at room temperature. Spectral absorption at 412 nm was measured and the free thiol content was calculated using the molar extinction coefficient of TNB (14,150 L mol^{-1} cm^{-1}) according to the manufacturer's instructions.

Antibody oxidation protocol

NISTmAb stock (10 g L^{-1}) and durvalumab stock (50 g L^{-1}) were first diluted to 4 g L^{-1} in PBS. To oxidize the antibodies, hydrogen peroxide (1% v/v) was added. Both control and oxidized samples were incubated for 48 h in the dark at room temperature. The samples were then buffer-exchanged into PBS using Zeba spin desalting columns (7-kDa MWCO). Samples were then stored at −20 °C until analysis. Buffer controls were performed using 25 mmol L^{-1} histidine buffer (pH 6.0) with and without the addition of hydrogen peroxide. The controls were diluted with PBS (pH 7.4) in an identical manner to experimental samples.

LC–MS/MS peptide mapping

Control and oxidized sample concentrations were diluted to 1.9 µg $µl^{-1}$ with denaturing buffer (5.4 mol L^{-1} guanidine HCl, 0.9 mmol L^{-1} EDTA and 90 mmol L^{-1} Tris, pH 7.8). Samples were reduced by adding DTT to a final concentration of 15 mmol L^{-1}, followed by incubation at 4 °C for 1 h. Samples were then alkylated by adding IAM to a final concentration of 29 mmol L^{-1}, followed by incubation at 4 °C for 1 h in the dark. Samples were exchanged to digestion buffer (1 mol L^{-1} urea in 0.13 mol L^{-1} Tris) using Zeba spin columns per the manufacturer's instructions. Trypsin was added to the samples for a final enzyme: IgG mass ratio of 1:18, followed by incubation at room temperature for 4 h. Finally, 0.1% formic acid was added at a 1:1 volume ratio to each sample. Digested samples were stored at −80 °C until analysis. Then, 5 µg of peptide digests were loaded using an autosampler onto a C18 column and analyzed by LC–MS. Peptide identification and quantification of methionine oxidation were performed using Genedata Expressionist version 15.0.6.

SASA analysis

Solvent-exposed areas of sulfurs in methionine residues in Protein Data Bank (PDB) 5K8A (the NISTmAb Fab, with five methionines) and PDB 5VGP (the NISTmAb Fc, with three methionines) were calculated by AREAIMOL in the CCP4 software suite[42], neglecting protein hydrogens and using default van der Waal radii. To account for flexibility, sulfur exposure numbers were averaged with their adjacent carbons and weighted for sequence proximity to peptide termini (only one methionine was close enough to affect its exposure value). The resulting structure-based estimates of peroxide exposure had a correlation of 0.87 with oxidation measurements (Supplementary Fig. 7d).

Detection of cysteine and antibody reduction by MEP

CV and CC measurements were taken using a CHI1040C electrochemical analyzer (CH Instruments). The measurements were performed with a three-electrode system containing a 2-mm-diameter glassy carbon working electrode, a Pt wire serving as the counter electrode and an Ag–AgCl reference electrode. For electrochemical measurement, samples were diluted to the appropriate concentration and then Fc (50 µmol L^{-1}) was added. For model amino acid studies, cysteine (50 µmol L^{-1} diluted in PBS) was used. For studies with fresh medium, NISTmAb (total mAb, 2 g L^{-1}) was spiked into AMBIC 1.1 basal medium. For studies with conditioned medium, NISTmAb (total mAb, 2 g L^{-1}) was spiked into spent Ex-Cell advanced fed-batch medium (cells removed) from a CHOZN23 (Millipore Sigma) cell culture. CV measurements were taken over a potential range of 0–0.5 V at a scan rate of 2 mV s^{-1}. CC measurements were taken at a constant potential of +0.4 V for 1 min and then switched to a reductive potential of +0.1 V for 1 min. All electrochemical measurements were taken from distinct samples. The working electrode was polished using 0.05 µm of alumina and rinsed with double-distilled H_2O between each measurement. All potentials are reported versus Ag–AgCl.

Detection of methionine and antibody oxidation by MEP

The electrochemical measurements were performed the same as above but with some modifications. Briefly, methionine and methionine sulfoxide (both at 2 mmol L^{-1} diluted in PBS) were used as the model amino acids. For antibody studies, NISTmAb and durvalumab samples were first diluted to the appropriate concentrations and then potassium hexachloroiridate(IV) (50 µmol L^{-1}) was added to samples. CV measurements were taken over a potential range of 0–0.85 V at a scan rate of 10 mV s^{-1}. CC measurements were taken at a constant input potential of +0.85 V for 1 min. All electrochemical measurements were taken from distinct samples. The working electrode was polished using 0.05 µm of alumina and rinsed with double-distilled H_2O between each measurement. All potentials are reported versus Ag–AgCl.

Statistics and reproducibility

Our experiments were performed on more than two dozen vials of NISTmAb (10 mg ml^{-1}) on more than 20 different occasions. The s.d. indicated represents more than five repeated sample preparations

from different vials, all prepared at the indicated concentrations. Statistical analysis was performed with Prism Graphpad and R version 3.4.3. Differences between intact and reduced or oxidized antibodies were assessed using the Mann–Whitney *U*-test (two-sided). A logistic regression model ('nnet' package) was used to assess the combination effect of multiple signal metrics for differentiating intact from reduced or control from oxidized mAbs. The AIC was used to estimate the quality of each model. The discriminating ability was evaluated using the ROC metric with the AUC (that is, *c* statistic) and *P* values.

Reporting summary

Further information on research design is available in the Nature Portfolio Reporting Summary linked to this article.

Data availability

The data supporting the findings of this study are available within the article and Supplementary Information. Raw data files are available are available from Zenodo (https://doi.org/10.5281/zenodo.13829075)[43]. Source data are provided with this paper.

References

41. Oliveira, S. C. B., Santarino, I. B. & Oliveira-Brett, A. M. Direct electrochemistry of native and denatured anticancer antibody rituximab at a glassy carbon electrode. *Electroanalysis* **25**, 1029–1034 (2013).
42. Winn, M. D. et al. Overview of the CCP4 suite and current developments. *Acta Crystallogr. D Biol. Crystallogr.* **67**, 235–242 (2011).
43. Motabar, D. et al. Detecting features of antibody structure through their mediator-accessible redox activities. *Zenodo* https://doi.org/10.5281/zenodo.13829075 (2024).

Acknowledgements

This work was supported by the Defense Threat Reduction Agency HDTRA1-19-1-0021 (to G.F.P. and W.E.B.), the Advanced Mammalian Biomanufacturing Innovation Center IUCRC2100632, 2004614245 (to W.E.B.) and the National Science Foundation MCB 2227598 (to G.F.P. and W.E.B.). This work was also supported in part by a Center of Excellence in Regulatory Science and Innovation grant to the University of Maryland from the US FDA 5U01FD005946-04 (to W.E.B.). This article reflects the views of the authors and should not be construed to represent the US FDA's views or policies. Identification of commercial materials and equipment does not imply recommendation or endorsement by the NIST. Figures were created in part with BioRender.com.

Author contributions

D.M., C.S., M.G., G.F.P. and W.E.B. designed the research. NIST researchers (T.M., T.D.G. and J.E.S.) guided the peroxide oxidation studies, performed MS and helped to interpret all methionine oxidation efforts (both NISTmAb and durvalumab), including interpretation and visualization. D.M., E.K., J.L. and Z.Z. contributed to the overall experimental methodology and execution of experiments. The preparation of figures and the manuscript, including final editing, was performed by D.M., T.M., T.D.G., M.G., C.S., G.F.P. and W.E.B.

Competing interests

The authors declare no competing interests.

Additional information

Supplementary information The online version contains supplementary material available at https://doi.org/10.1038/s41589-024-01778-z.

Correspondence and requests for materials should be addressed to Gregory F. Payne or William E. Bentley.

Peer review information *Nature Chemical Biology* thanks Lital Alfonta and the other, anonymous reviewers for their contribution to the peer review of this work.

nature portfolio

Corresponding author(s): William E. Bentley

Last updated by author(s): 09/18/2024

Reporting Summary

Nature Portfolio wishes to improve the reproducibility of the work that we publish. This form provides structure for consistency and transparency in reporting. For further information on Nature Portfolio policies, see our Editorial Policies and the Editorial Policy Checklist.

Statistics

For all statistical analyses, confirm that the following items are present in the figure legend, table legend, main text, or Methods section.

n/a	Confirmed
☐	☒ The exact sample size (*n*) for each experimental group/condition, given as a discrete number and unit of measurement
☐	☒ A statement on whether measurements were taken from distinct samples or whether the same sample was measured repeatedly
☐	☒ The statistical test(s) used AND whether they are one- or two-sided *Only common tests should be described solely by name; describe more complex techniques in the Methods section.*
☒	☐ A description of all covariates tested
☒	☐ A description of any assumptions or corrections, such as tests of normality and adjustment for multiple comparisons
☐	☒ A full description of the statistical parameters including central tendency (e.g. means) or other basic estimates (e.g. regression coefficient) AND variation (e.g. standard deviation) or associated estimates of uncertainty (e.g. confidence intervals)
☒	☐ For null hypothesis testing, the test statistic (e.g. *F*, *t*, *r*) with confidence intervals, effect sizes, degrees of freedom and *P* value noted *Give P values as exact values whenever suitable.*
☒	☐ For Bayesian analysis, information on the choice of priors and Markov chain Monte Carlo settings
☒	☐ For hierarchical and complex designs, identification of the appropriate level for tests and full reporting of outcomes
☒	☐ Estimates of effect sizes (e.g. Cohen's *d*, Pearson's *r*), indicating how they were calculated

Our web collection on statistics for biologists contains articles on many of the points above.

Software and code

Policy information about availability of computer code

Data collection	CHI1040C Electochemical Analyzer software, Agilent 2100 Expert software (Revision B.02.06)
Data analysis	GraphPad Prism Version 8.0.2, and R version 3.4.3, Microsoft Excel

For manuscripts utilizing custom algorithms or software that are central to the research but not yet described in published literature, software must be made available to editors and reviewers. We strongly encourage code deposition in a community repository (e.g. GitHub). See the Nature Portfolio guidelines for submitting code & software for further information.

Data

Policy information about availability of data

All manuscripts must include a data availability statement. This statement should provide the following information, where applicable:

- Accession codes, unique identifiers, or web links for publicly available datasets
- A description of any restrictions on data availability
- For clinical datasets or third party data, please ensure that the statement adheres to our policy

The authors declare that the data supporting the findings of this study are available within the paper and its Supplementary Information file. Raw data files are available upon request and are provided online.

Human research participants

Policy information about studies involving human research participants and Sex and Gender in Research.

Reporting on sex and gender	N/A
Population characteristics	N/A
Recruitment	N/A
Ethics oversight	N/A

Note that full information on the approval of the study protocol must also be provided in the manuscript.

Field-specific reporting

Please select the one below that is the best fit for your research. If you are not sure, read the appropriate sections before making your selection.

☒ Life sciences ☐ Behavioural & social sciences ☐ Ecological, evolutionary & environmental sciences

For a reference copy of the document with all sections, see nature.com/documents/nr-reporting-summary-flat.pdf

Life sciences study design

All studies must disclose on these points even when the disclosure is negative.

Sample size	Sample sizes were determined based upon the number of samples that were required to produce a statistically significant response using the Mann-Whitney test for the reduced and oxidized samples, respectively.
Data exclusions	No data was excluded.
Replication	To verify reproducibility, samples were analyzed across multiple sample treatments and across multiple days. Our experiments were performed on greater than 2 dozen vials of NISTmAb (10mg/mL)on more than 20 different occasions and showed repeatability.
Randomization	Antibody samples were allocated based upon sample treatment. Antibodies that had undergone the reduction protocol were labeled as 'reduced'. Antibodies that had undergone the oxidation protocol were labeled as 'oxidized'.
Blinding	Blinding was not relevant to this study as the the protocol and parameters for the electrochemical measurements were standardized for each respective sample type (intact and reduced samples; control and oxidized samples).

Reporting for specific materials, systems and methods

We require information from authors about some types of materials, experimental systems and methods used in many studies. Here, indicate whether each material, system or method listed is relevant to your study. If you are not sure if a list item applies to your research, read the appropriate section before selecting a response.

Materials & experimental systems

n/a	Involved in the study
☐	☒ Antibodies
☒	☐ Eukaryotic cell lines
☒	☐ Palaeontology and archaeology
☒	☐ Animals and other organisms
☒	☐ Clinical data
☒	☐ Dual use research of concern

Methods

n/a	Involved in the study
☒	☐ ChIP-seq
☒	☐ Flow cytometry
☒	☐ MRI-based neuroimaging

Antibodies

Antibodies used	NISTmAb RM8671 (Lot 14HB-D-002, humanized IgG1κ) was obtained from National Institute of Standards of Technology (NIST). Durvalumab (MedImmune/AstraZeneca) was purchased via McKesson Specialty Health (Scottsdale, Arizona) and samples for our study were obtained from the FDA.. Durvalumab is commercially available by prescription only.

Validation	NISTmAB was validated by NIST. Further information can be found at the NIST website: https://www.nist.gov/programs-projects/nist-monoclonal-antibody-reference-material-8671 Durvalumab was validated by MedImmune/AstraZeneca. Further information can be found at the FDA website: https://www.accessdata.fda.gov/drugsatfda_docs/label/2022/761069s035lbl.pdf